Electronic structure and thermodynamics of defects in $NiAl_3$

M. Rasamny
Department of Computer and Information Science, Delaware State University, Dover, Delaware 19901 and U-46, Physics Department, University of Connecticut, Storrs, Connecticut 06269

M. Weinert
Department of Physics, Brookhaven National Laboratory, Upton, New York 11973

G. W. Fernando
U-46, Physics Department, University of Connecticut, Storrs, Connecticut 06269 and Institute of Fundamental Studies, Hantana Road, Kandy, Sri Lanka

R. E. Watson
Department of Physics, Brookhaven National Laboratory, Upton, New York 11973
(Received 15 May 2001; published 21 September 2001)

We present first-principles calculations of the structural and electronic properties of orthorhombic $NiAl_3$, including the intrinsic point defects. The energies obtained from these calculations are employed in a statistical mechanics model to investigate the role of $NiAl_3$ in the Ni-Al phase diagram. Our calculations show that the preferred constituent defect mechanisms for $NiAl_3$ off stoichiometry are the $8d$ Ni antisites on the Ni-rich side and Ni vacancies on the Al-rich side. The calculated free energy is in agreement with the observation that $NiAl_3$ is a stoichiometric compound.

DOI: 10.1103/PhysRevB.64.144107 PACS number(s): 61.72.Ji, 61.66.Dk, 64.60.Cn, 71.15.Mb

I. INTRODUCTION

Intermetallics such as Ni-Al have emerged as a promising class of materials that may be developed for use in harsh environments containing corrosive gases and operating at high temperatures and large stresses. Of primary importance when attempting to engineer the properties of intermetallics is an understanding of the equilibrium and metastable phases and their ranges of stability with respect to composition and temperature. A detailed understanding of the phase diagram at and about stoichiometry is necessary if one wishes to proceed further. Such a direction has and continues to be actively pursued at both the experimental and theoretical levels. In the case of Ni-Al alloys, the emphasis has been on the Ni-rich and ordered $B2$ (bcc) compounds. The Al-rich Ni-Al alloys, on the other hand, have received little attention, in part due to their low melting temperatures and the difficulties associated with their synthesis. The Al-rich phases, however, represent an integral part of the Ni-Al phase diagram and studying these systems contributes to our fundamental understanding of the role they play in the Ni-Al phase diagram and to possible technological contributions. The Al-rich side of this system possesses two ordered phases: $NiAl_3$ which forms in a complex 16-atom orthorhombic primitive cell and Ni_2Al_3. In this paper, we will concentrate on the former. The ability for a phase to remain stable at concentrations away from stoichiometry implies that a coexistence of intrinsic point defects—antisites and vacancies—within the system is energetically favorable. Therefore, a thorough understanding of the $NiAl_3$ system and its role in the Ni-Al phase diagram must begin with an investigation of the pure system and its intrinsic point defects. There are several factors which will be seen to be important to the energetics of defect formation. One is that Al has a larger elemental volume than does Ni and accommodating Al's larger size is sometimes energetically costly. Another factor is that Ni and Al like to bond and those defects which act to increase the number of Al-Ni near-neighbor pairs tend to be energetically favorable. In addition, lattice relaxations around the defects may be energetically significant.

Since both Ni and Al are fcc and NiAl is bcc like, the $NiAl_3$ system naively might be expected to form in a structure closely related to a decorated fcc or bcc lattice; however, this is not the case. Instead, it forms in the cementite CFe_3 (DO_{11}) structure, which is a primitive orthorhombic structure with 16 atoms ($oP16$) in the unit cell. The system has a low melting temperature of around 854 °C and is unstable away from stoichiometry. Experimental work on this material is relatively rare, although the density of states of has been measured using Al $KL_{23}V$ and Ni LMM Auger spectroscopy and valence-band x-ray photoemission spectroscopy[1,2] (XPS), and x-ray-absorption fine structure (XAFS) above the Ni K edge.[3] Electronic structure calculations have been done[4,5] employing the reported lattice parameters for the structure but these did not estimate the heat of formation. Calculations pertaining to the Ni-Al system have also been done where $NiAl_3$ has been represented by the fcc-based Cu_3Au, $cP4$ ($L1_2$)structure[6,7] since the small size and high symmetry of this structure render it computationally more tractable. According to our calculated heats of formation, the correct $NiAl_3$ structure is favored by about 0.2 eV/atom (-0.46 vs -0.26 eV/atom) over the Cu_3Au structure, a significant difference.

First-principles calculations allow us to probe the electronic structure of defects in $NiAl_3$ and provide, to a certain degree, information about the role of $NiAl_3$ in the Ni-Al

phase diagram. To better describe such a role requires a thermodynamic approach that allows these defects to coexist in the system. This is implemented here via a statistical mechanical method that utilizes information about the energetics obtained from first-principles pseudopotential calculations of those intrinsic point defects.

II. FIRST-PRINCIPLES CALCULATIONS

The $oP16$ (DO_{11}) structure has three inequivalent sites: Ni $4c$, Al $4c$, and Al $8d$ with internal parameters not determined by symmetry. $NiAl_3$, therefore, has six simple intrinsic defects: vacancies on the Ni and two Al sites, two Ni antisites (on the Al $4c$ and $8d$ sites), and an Al antisite on the Ni site. Also, a thorough examination of the $NiAl_3$ structure reveals sites in the interstitial region close to $(0,0,\frac{1}{2})$ that are, based on the calculations and on size effect analysis, auspicious for Ni but not for Al. The actual calculated position of such a Ni interstitial is slightly off of the $4b$ site appropriate to the symmetry of this structure: this position was chosen by searching for a site that could accommodate an interstitial. (We do not consider an Al interstitial because Al too large to be accommodated at this site.)

The first-principles calculations use an iterative plane-wave pseudopotential[8] method. An important issue when dealing with such methods is the construction of transferable pseudopotentials that perform well in various alloy environments. In Appendix A, we discuss the generation of transferable Ni and Al pseudopotentials. The idea is to recognize that pseudopotentials are approximations to all-electron calculations. By exploiting the arbitrariness inherent in pseudopotentials, the pseudopotentials can be optimized so as to reproduce all-electron results as well as possible. Proceeding along these lines, Appendix A provides evidence of the transferability of the Ni and Al pseudopotentials by comparing results with all-electron calculations for various simple alloys.

To calculate defects using first-principles methods that utilize periodic boundary conditions, it is often necessary to use supercells. In principle, the cell should be chosen large enough so that the interactions felt by the defect due to its images in neighboring cells are negligible. For methods that utilize plane waves, the size of the cell is also dictated by the cutoff energy. Ni, being one of the more difficult $3d$ transition elements, requires a large energy cutoff that restricts the size of the system that can be treated. For most of the atomic defect calculations in $NiAl_3$ discussed in this paper, we restricted the system to the primitive (16-atom) cell; for a few test cases, the (Ni-rich) Ni $8d$ antisite and the (Al-rich) Ni vacancy, we used 32- and 64-atom supercells. The resulting energy changes in the calculated energies of the defects (the parameters ε_{8d}^{Al} and ε_{v}^{Ni}) were approximately 0.01–0.015 eV, and the change on going to the 64-atom cell from the 32-atom one for the Ni $8d$ antisite was less than 0.006 eV. The changes in the relaxations of the nearest-neighbor shell of atoms compared to the 16-atom cell were less than 0.02 a.u. Other defects that we expect (based on our calculations) to have a larger size dependence are much higher in energy even with reasonable estimates of the increased relaxation. Thus, these defects are not expected to play a major role in the thermodynamics and we have limited our consideration to the small cell.

TABLE I. Experimental (Ref. 11) and calculated internal structural parameters for $NiAl_3$. The experimental (calculated) lattice parameters are $a=12.300$ (12.309) a.u., $b=13.707$ (13.717) a.u., and $c=8.951$ (8.957) a.u.

	Experimental			Optimized		
Atom type	x	y	z	x	y	z
Ni	−0.131	$\frac{1}{4}$	0.945	−0.130	$\frac{1}{4}$	0.944
Al ($4c$)	0.011	$\frac{1}{4}$	0.415	0.007	$\frac{1}{4}$	0.417
Al ($8d$)	0.174	0.053	0.856	0.171	0.055	0.864

For exchange correlation, the parametrization of Vosko, Wilk, and Nusair[9] was used. For the $oP16$ structure of $NiAl_3$, 64 special k points[10] were used in the irreducible Brillouin zone. For vacancies and impurities on the $4c$ and $8d$ sites, this number increased to 128 and 256 special points, respectively, because of the lowered symmetry. For each of the defect calculations presented here, full structural relaxations of the volume and all internal parameters were done.

A. Pure $NiAl_3$

Both the lattice constants and the internal coordinates of the different species of atoms, Table I, were determined variationally and the agreement with experiment[11] is very good. The heat of formation is calculated to be $\Delta H=-0.46$ eV/atom. Although less in magnitude than the calculated ΔH for the more Ni-rich compounds, it is stable against a two-phase mixture of these and pure Al.

The calculated density of states (DOS) is given in Fig. 1.

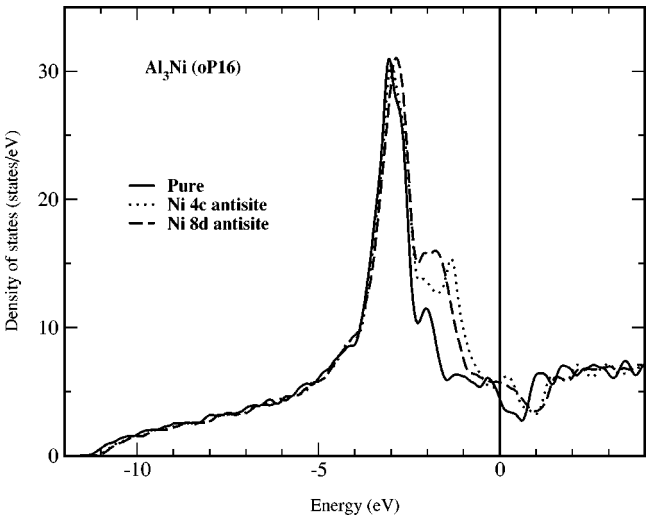

FIG. 1. Density of states for the pure $NiAl_3$ phase and for the two systems with the Ni antisite defects. Note the increased intensity and broadening of the high-energy shoulders close to the Fermi level for the defect calculations resulting from an increase in the Ni-Ni interactions.

The width of the high density of states peak is of the order of the width associated with an isolated Ni atom in aluminum. The shoulder closer to the Fermi level is associated with Ni-Ni d electron interactions. The observed XPS valence-band spectra[1,2] shows the narrow and sharp $3d$ Ni bands peaking around -3.0 eV, in agreement with our calculations. The shoulder in the DOS nearer the Fermi level is also prominent in the experiment, although its position varies[1,2] depending on the experiment.

B. Defects in fcc Al

The formation energy of a vacancy in fcc Al was calculated previously,[8] $\Delta H_v = +0.66$ eV (the plus sign indicating that it is energetically unfavorable). In the present paper, a Ni impurity in Al has a calculated $\Delta H_f = -0.94$ eV (relative to spin-polarized Ni). This heat is substantial and binding, indicative of the fact that defects that increase the number of Ni-Al nearest-neighbor pairs will benefit energetically from the Ni-Al bonding. If the energetics of higher concentrations of Ni in Al can be modeled as a sum of the single-impurity heats, i.e., assuming the Ni defects do not interact, then at $x=0.25$, the heat of formation of the resulting "$NiAl_3$" would be -0.24 eV/atom, compared to the calculated (fcc) Cu_3Au value of -0.26 eV/atom. This close agreement suggests that even at high densities, the (direct and indirect) interactions among Ni atoms are small. As noted above, however, the $oP16$ structure has a larger heat of -0.46 eV/atom, so that Ni is insoluble in Al and a two-phase regime of Al and $NiAl_3$ wins out for dilute Ni concentrations.

C. Defect heats at $T=0$

Calculated defect heats (Gibbs free energies at $T=0$) are shown in Fig. 2, where they are plotted as a function of the effective alloy concentration. Comparison of the relative energetics of different defects can meaningfully be done by comparing the energies associated with different defects at some chosen alloy composition, assuming that defect-defect interactions are small. Note that all the defects, except the $8d$ Ni antisite, cost energy; i.e., they lie above the heat of the stoichiometric compound.

Figure 2 also illustrates the importance of including the heats of competing phases. Stability of a system off stoichiometry is possible only if there is at least one defect that is energetically more favorable than a two-phase mixture. As noted above, the heat of formation of the $8d$ Ni antisite is more bound than that of the ideal $oP16$ structure. This does not mean that this defect system will form; rather, competition with other phases must be considered. The position of the tie line relative to the antisite ΔG indicates that the $8d$ Ni antisite is unstable (at $T=0$) relative to a two-phase mixture of $NiAl_3$ and Ni_2Al_3.

D. Size effects in Al-rich defects

The only two Al-rich defects are Al antisites and Ni vacancies. Of the two, Ni vacancies are stabler, as seen in Fig. 2. Size effects play a significant role: the Ni bond length is about 13% smaller (33% in atomic volume) than Al. The Ni-Al bond lengths are shorter in length than the Al-Al bonds in fcc Al, so that creation of an Al antisite, i.e., the replacement of the smaller Ni atom by a larger Al atom, results in a situation that is energetically unfavorable unless the (antisite) Al-Al bond lengths are allowed to increase. This process is clearly occurring in Fig. 3 where the top

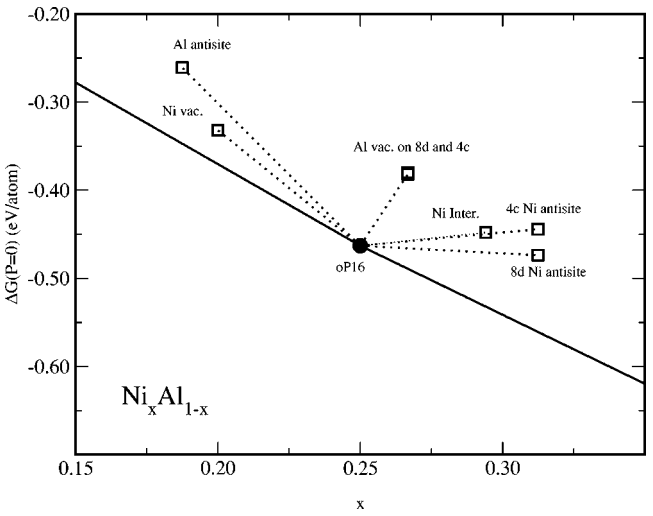

FIG. 2. Calculated heats of formation (Gibbs energies) at $T=0$ $NiAl_3$ with various defects. The squares represent the results of the first-principles calculations at the concentration due to the introduction of the defect into the calculational cell, and the solid lines are tie lines representing two-phase mixtures at $T=0$ of Al and $NiAl_3$ ($x<0.25$) and of $NiAl_3$ and Ni_2Al_3 ($x>0.25$). The dotted lines represent the concentration dependence of the system with a particular defect, assuming interactions among defects are negligible. Note that the Ni $8d$ antisites and Ni vacancies are preferred over the other defects; however, all defects except the Ni $8d$ antisite have a smaller $|\Delta H|$ than the ideal system.

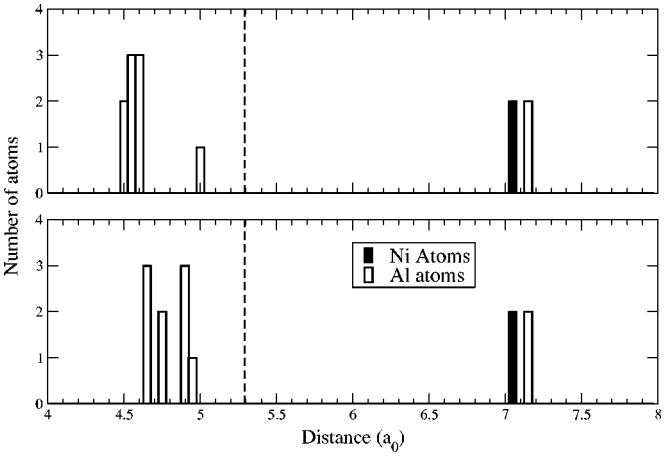

FIG. 3. Ni and Al neighbors as seen by the Al atom sitting on a Ni site in the pure $oP16$ structure (top) and after structural relaxation (bottom). The dashed vertical line represents the Al-Al distance in the elemental solid. Notice the outward movement in the first shell of neighbors, and the lack of movement in the second shell of neighbors, indicating a significant screening of the defect by the inner shells.

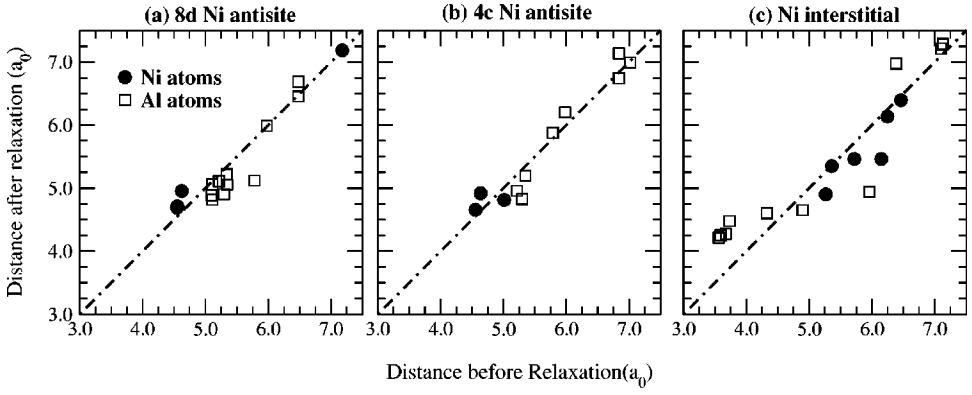

FIG. 4. Near neighbor distances around the (a) Ni $8d$ antisite, (b) Ni $4c$ antisite, and (c) Ni interstitial defect before vs after relaxation. Atoms below (above) the diagonal indicate movement toward (away) from the defect. The Ni $8d$ antisite, Ni $4c$ antisite, and Ni interstitial have 9(3), 10(3), and 9(4) Al(Ni) neighbors, respectively. Unlike (a) and (b), the Ni interstitial shows a great deal of movement in the outer atomic shells, indicating significant interactions with the defect.

radial distribution shows the neighborhood of the Al antisite before relaxation in the $oP16$ structure and the bottom plot shows the neighborhood after relaxation. It is clear that there is significant outward relaxation of the inner Al shells of neighbors closer than $5a_0$, while the Ni and Al atoms farther away show little movement. The outward relaxation still has not brought the Al-Al bond lengths close to those in Al metal and this size effect contributes to the preference of the Ni vacancy over the Al antisite. The lack of movement in the second shell of neighbors in Fig. 3 indicates that the primitive cell is providing enough of an isolated environment to prove adequate for this defect calculation. (For this case, larger cells were calculated with similar results.)

E. Dominant effects in Ni-rich defects

From Fig. 2 it is seen that Al vacancies are not competitive in the Ni-rich regime. As for the Ni antisite and interstitial defects, the question of relaxation effects arise and these are plotted in Fig. 4. The $8d$ and $4c$ Ni antisite have 9(3) and 10(3) Al(Ni) neighbors, respectively, while the Ni interstitial has 9(4) Al(Ni) neighbors. The nearest-neighbor distances in the Ni interstitial are around $3.6a_0$, which is too small to accommodate an Al interstitial defect. In the figure, points falling on the diagonal line indicate no atomic movement associated with relaxation, while points falling above or below the line indicate movement away or towards the Ni atom, respectively. Both the $8d$ and $4c$ sites have an equal number of Ni neighbors, and although not obvious, the $4c$ site has six Al atoms at a distance of less than $5.5a_0$, while for the Ni interstitial defect, there are seven Al atoms. Three things are worth noting about these graphs.

First, the presence of the Ni atom at the $8d$ and $4c$ defect sites forms energetically favorable Ni-Al bonds, as indicated by the inward motion of the Al atoms surrounding the Ni defect. This effect is more pronounced for the $8d$ Ni antisite where the coordination is also increased by one because of a relatively large ($0.70a_0$) contraction of a Ni-Al bond. The 0.56 and 0.41 eV relaxation energies are a reflection of the wide range of motion observed in the $8d$ and $4c$ Ni antisites, respectively. Without these relaxations, the $4c$, rather than the $8d$, would be the stabler of the two antisites. In the case of the Ni interstitial, the presence of the Ni atom forms very short and, therefore, highly unfavorable Ni-Al bonds that result in an outward relaxation of the Al atoms surrounding the interstitial.

Second, a Ni atom at an antisite is, as is to be expected, actively involved in d bonding with its Ni neighbors. Evidence for this can be seen in the densities of states shown in Fig. 1. Compared to the pure system, the narrow double d peak becomes wider with the antisite present. Inspection of local, site-specific DOS (not shown here) indicates antisite wave function character mixed in throughout the double-peak structures. The $4d$ site shows the greater splitting of the higher-lying shoulder; although this may indicate greater mixing, it does not guarantee larger energy stabilization.

Third, there is evidence of strong screening of the presence of the $8d$ Ni antisite in Fig. 4(a): there is a large relaxation of the closer Al shells and almost no effect on the farther out shells. The effect is similar to what was observed earlier for the Al antisite defect, and it is unlikely that a significant further energy improvement will be obtained upon going to a larger (e.g., 32- or 64-atom) cell. The screening effects are not as strong for the $4c$ Ni antisite in Fig. 4(b) since there is still some relaxation to be seen in the outer Al shells. Such motion is also seen to a greater degree in the outer shells of the Ni interstitial defect in Fig. 4(c). A comparison with the other figures quickly reveals a failure to achieve the optimal Ni-Al bond lengths in the Ni interstitial. A supercell calculation for this defect may allow this defect system to better approach the optimal Ni-Al bond lengths but it is still not expected to compete energetically with the antisites since an additional relaxation energy of ~ 0.38 eV would be required; based on our calculations, such a large energy gain is unlikely.

III. THERMODYNAMICS OF $NiAl_3$

The first-principles calculations presented above provide details on the electronic structure and energetics of defects in $NiAl_3$ at $T=0$. We are now in a position to use this information to describe a homogeneous thermodynamically stable

TABLE II. Low-temperature defect formation energies (in eV) for various defects for different concentrations around $NiAl_3$ [cf. Eq. (B10) in Appendix B]. The constituent defects ($\Delta H \equiv 0$) are the Ni vacancy for Al-rich systems and the Ni $8d$ antisite for Ni-rich systems.

	Ni sites		Al $8d$ sites		Al $4c$ sites		Inter.
	ΔH_v^{Ni}	ΔH_{Al}^{Ni}	ΔH_v^{Al}	ΔH_{Ni}^{Al}	ΔH_v^{Al}	ΔH_{Ni}^{Al}	ΔH_{Ni}^{I}
Al-rich	0	0.61	1.90	2.44	1.90	2.90	2.22
$NiAl_3$	1.05	2.01	1.55	1.05	1.56	1.50	1.18
Ni-rich	1.83	3.06	1.29	0	1.29	0.45	0.39

system. Such studies have been successfully carried out on NiAl and other $B2$ compounds.[12,13] Unlike those systems, the equations describing the thermodynamics of $NiAl_3$ are more complicated and must be extended.

In a homogeneous thermodynamically stable system, various defects must coexist in order to maintain concentration. If we assume that the system under consideration contains a low concentration of defects, then a noninteracting statistical mechanical model can be developed, as explained in Appendix B, that describes a system in thermodynamic equilibrium with its defects. By minimizing an ansatz for the Gibbs free energy with respect to the number of defects, we obtain expressions for the defect concentration, Eqs. (B3)–(B6). These expressions contain parameters ε_i^ν and v_i^ν that represent the difference in energy and volume, respectively, between a cell containing a defect and an ideal cell. Since the volumes have been relaxed ($P=0$) in the first-principles calculations, all the Pv_i^ν terms in the free energy drop out. Furthermore, we will use the energetics furnished by the first-principles calculations of the previous section to obtain the ε_i^ν parameters. This is an acceptable approximation as long as the cells used in the first-principles calculation are large enough for defect-defect interactions to be small. Once these parameters have been calculated, the equations for the defect concentrations along with other constraints imposed on the system are solved for the chemical potentials of the constituent atoms and then the formation energies of the thermally activated defects can be found.

A. Defect formation energies in $NiAl_3$

Table II gives the defect formation energies ΔH_i^ν at low temperature. The superscript describes the site or sublattice involved in the defect and the defect atom is indicated by the subscript. For example, ΔH_{Al}^{Ni} is the defect formation energy for an Al atom going to the Ni sublattice, i.e., an Al antisite. In order to satisfy a concentration off stoichiometry, certain defects remain even as $T \to 0$. These constitutional—or structural—defects have by definition defect formation energies $\Delta H_i^\nu = 0$, as can easily be deduced from Eqs. (B3)–(B6). For $NiAl_3$ (cf. Table II), the constitutional defects are Ni vacancies on the Al-rich side ($x<0.25$) and $8d$ Ni antisites on the Ni-rich side ($x>0.25$). This same conclusion may also be deducted from Fig. 2, where the heats of formation at $T=0$ favor these two defects.

TABLE III. Defect formation energies for possible stoichiometric complexes at $x=0.25$ in $NiAl_3$. The numbers in parentheses indicate the size of the complex.

Defect complexes	ΔH_i^ν (eV/defect)
(7) 4 Ni vacancy $+3$ $8d$ Ni antisites	1.05
(2) Ni vacancy + Ni interstitial	1.11
(7) 4 Ni vacancy $+3$ $4c$ Ni antisites	1.24
(4) Ni vacancy $+3$ $8d$ Al vacancy	1.43
(4) Ni vacancy $+3$ $4c$ Al vacancy	1.43
(7) 3 Al antisite $+4$ Ni interstitial	1.53
(2) Al antisite $+8d$ Ni antisite	1.53
(5) Al antisite $+4$ $8d$ Al vacancy	1.64
(5) Al antisite $+4$ $4c$ Al vacancy	1.65
(2) Al antisite $+4c$ Ni antisite	1.76

For Ni-poor concentrations $x<0.25$, Table II puts the Al antisite at 0.61 eV above the Ni vacancy. As was discussed earlier, this energy difference involves both bonding and size effects. The rest of the defects are still higher-lying excitations, demonstrating the fact that creation of Ni-rich defects in an Al-rich environment is energetically undesirable.

For Ni-rich concentrations $x>0.25$, the Ni interstitial and $4c$ Ni antisite lie very close to each other (Fig. 2), both lying 0.4 eV higher in energy than the Ni $8d$ antisite. No clear distinction can be made about which defect is energetically more favorable since their defect formation energies are close enough to lie within the error bars of this calculation. The Al vacancies, the remaining only two Ni-rich defects, are seen to be highly unstable, as expected from Fig. 2.

At stoichiometry, the defect formation energies for the constitutional defects must be equal; were this not the case, the system would be unable to maintain its stoichiometry, producing more of one defect and promoting instability. At $T=0$, it can be shown analytically that the defect formation energies for the constitutional defects are given by

$$\Delta H_v^{Ni} = \Delta H_{Ni}^{8dAl} = \frac{1}{28}(E_0 + 16\varepsilon_v^{Ni} + 12\varepsilon_{Ni}^{8dAl}), \qquad (1)$$

where E_0 is the energy per unit cell of the pure $oP16$ structure. In order to maintain stoichiometry, both Ni vacancies and $8d$ Ni antisites must be formed; three $8d$ Ni antisites must be formed somewhere in the system whenever four Ni vacancies are created.

This ''septuplet'' Ni-vacancy/$8d$-Ni-antisite complex is not the only possible defect complex that can be formed at $NiAl_3$ stoichiometry. In contrast with the bcc-based $B2$ compounds, the defect complexes that can occur in $NiAl_3$ are more complex and greater in number because of the different stoichiometry. The simplest of these complexes involve pairs of defects: a Ni vacancy and Ni interstitial and an Al antisite combined with either the $4c$ or the $8d$ Ni antisite. Table III shows that these simple defect complexes are not as energetically favorable as the septuplet Ni-vacancy/$8d$-antisite complex. However, the energies are close enough that it is not possible to unambiguously discern whether $NiAl_3$ is a binary or septuplet defect system.

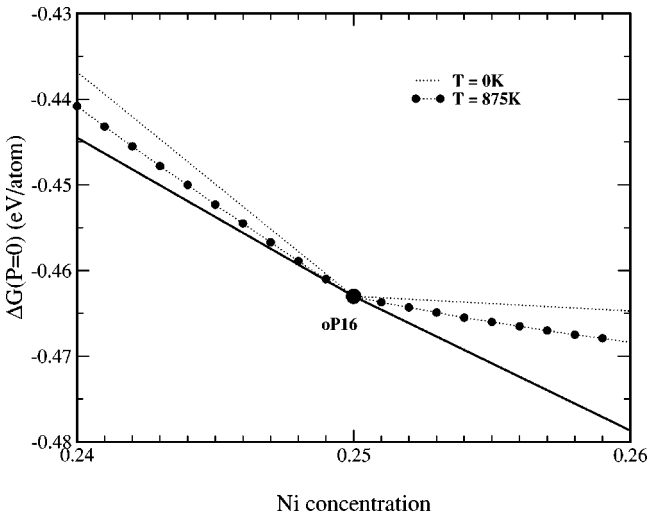

FIG. 5. Calculated free energies for $NiAl_3$ at $T=0$ and $T=875$ K. The $T=0$ tie lines (solid lines) are also shown.

The defect formation energies also give insight into the ability of the system to maintain order at high temperature. If the defect formation energies are small and the melting temperature is high enough, disorder is expected to set in as the melting temperature is approached. According to Tables II and III, the defect formation energies at stoichiometry are all above 1 eV. Since $NiAl_3$ has a low melting temperature of 854 °C, it is expected to remain a well-ordered system as the melting temperature is approached.

B. Free energy of $NiAl_3$

Although we have shown that the defects required to accommodate off stoichiometry in in $NiAl_3$ are unstable relative to a two-phase mixture at $T=0$, this may change as the temperature increases and entropy contributes to the free energy. Consider the calculated Gibbs free energies shown in Fig. 5 for $NiAl_3$ at both $T=0$ and $T=875$ K. Vibrational entropies have been omitted from the calculated energies, which is expected to have only a modest effect on the results. The solid lines are the $T=0$ tie lines; note that the tie lines are temperature dependent and represent the competing two-phase mixture.

The $T=0$ Gibbs free energy has a break in slope at $x=0.25$ and there are breaks in defect formation energies as seen in Table II, associated with the discontinuous behavior of the Ni and Al chemical potentials. (Since the chemical potentials describe the energy required to add or remove an atom, they must take on different values for $x<0.25$ and $x>0.25$ because of the different constituent defects there; the chemical potentials to either side will remain constant as a function of concentration at $T=0$ since only one type of defect, the constitutional defect, exists.) Note that the Gibbs free energy can be written as $G=(\mu_{Ni}-\mu_{Al})x+\mu_{Al}$ in terms of the chemical potentials and the Ni concentration x. Although the chemical potentials are temperature and concentration dependent, at zero temperature $d\mu_i/dx$ $(T=0)=0$ and the slope of the free energy curve is the difference in the chemical potentials $\mu_{Ni}-\mu_{Al}$. The existence of a Ni vacancy as the constitutional defect on the Al-rich side makes this difference larger in magnitude as seen in Fig. 5 compared to the same on the Ni-rich side.

Going to nonzero temperatures, a population of thermally activated defects develops and the Gibbs free energy becomes more negative on either side of $x=0.25$ due to the configurational (and other) entropy term. Because at higher temperatures the chemical potentials are concentration dependent, the Gibbs free energy (versus concentration) curves acquire curvature. Hence, the slope of the free energy curve is continuous at $x=0.25$, unlike at $T=0$. However, such smooth behavior is not discernible in Fig. 5 for $T=875$ K because of the high activation energies; the lowest activation energy in Table II is 0.39 eV (corresponding to 4500 K). (Note that these activation energies are also temperature dependent, but the scale is still large.) The result is that for all temperatures up to melting, the tie lines effectively intercept at $x=0.25$, implying that $NiAl_3$ is a line compound throughout.

IV. CONCLUSION

Using first-principles calculations, we have investigated the electronic structure and properties of lattice defects in $NiAl_3$. Ni-Al bonds contribute substantially to the binding of the alloy, and defects that are able to increase the number of Ni-Al bonds (at the ''natural'' bond length) benefit from such configurations. This increase in binding is quite apparent in some of the Ni-rich defects, especially the $8d$ and $4c$ Ni antisite defects. A Ni interstitial increases the number of Ni-Al pairs but the bond lengths are far from optimal, causing a decrease in bonding. Had the bond lengths been close to the natural bond lengths (with the same number of Ni-Al pairs), then this defect would have expected to be more competitive with the Ni antisite.

In terms of relative stability of the various defects, size effects play a major role in the Al-rich $NiAl_3$ systems. In that case, size mismatch between the Ni and Al favors Ni vacancies over Al antisites. In Ni-rich $NiAl_3$, the large relaxation energy (0.56 eV) associated with the $8d$ Ni antisite, along with the loss of bonding associated with the Al vacancy, leads to the $8d$ antisite defect being the most stable. This result illustrates that relaxations around the defects are important and must be considered in defect calculations.

Using a thermodynamic approach, information about defect structure of $NiAl_3$ was obtained. By calculating the defect formation energies, the defect mechanisms that might exist both off and on stoichiometry were obtained. These formation energies are large, about 1 eV, thus yielding low defect concentrations at normal temperatures. There is no strong preference for any particular defect complex at stoichiometry and no strong site preference off stoichiometry. From the calculated free energy as a function of concentration, we find that $NiAl_3$ has a small stoichiometry range all the way up to its melting temperature.

ACKNOWLEDGMENTS

This work was supported in part by the Division of Materials Sciences, U.S. Department of Energy, under Contract

No. DE-AC02-98CH10886, the Research Foundation at the University of Connecticut, and by a grant of computer time at the National Energy Research Scientific Computing Center. We thank Professor J. Budnick and Professor D. Pease for helpful discussions.

APPENDIX A: Ni AND Al PSEUDOPOTENTIAL CONSTRUCTION

In first-principles pseudopotential methods, one is often confronted with the issue of transferability and stability of the pseudopotentials, especially in alloys. It has been demonstrated[14] that wrong structures may be predicted using many of the common pseudopotential constructions for a wide range of inputs. The pseudopotential construction technique[14,15] implemented here cuts off the pseudopotential in reciprocal space and is adjusted to reproduce all-electron results for a number of different crystal structures. The resulting pseudopotentials are both stable and transferable.

The starting pseudopotentials are generated using the Troullier-Martins scheme[16] and put into a separable form using a Kleinman-Bylander procedure.[17] The all-electron calculations used to ''tune'' the pseudopotentials were performed using the full-potential linearized augmented Slater-type orbital (LASTO) method.[18] The Al pseudopotential is the same as used previously.[8]

Ni, being near the end of the transition metal row, has a localized $3d$ orbital, resulting in a very deep pseudopotential. Using various pseudopotential cutoffs ranging from $E_{ps}=55$ Ry to $E_{ps}=72$ Ry and plane-wave cutoffs ranging from $E_{cut}=E_{ps}$ to $E_{cut}=75$ Ry, we investigated the convergence of the total energy in a bulk Ni fcc environment. For $E_{cut}-E_{ps}\approx 5$ Ry the total energy is converged to within 1 meV. Structural parameters such as lattice constant and bulk modulus for both fcc and bcc Ni were closest to the all-electron values for $E_{ps}=65$ Ry. However, at this cutoff, the fcc-bcc structural energy difference was not satisfactory. Choosing $E_{ps}=72$ Ry and $E_{cut}=75$ Ry for our Ni pseudopotential yielded structural parameters and an fcc-bcc energy difference that were in excellent agreement with the all-electron results.

As a check on the transferability of the Ni and Al pseudopotentials generated for the calculations presented in this paper, the structural properties and heats of formation of three different Ni-Al alloys—fcc-based $NiAl_3$ in the $L1_2$ (Cu_3Au) structure, hexagonal Ni_2Al_3 ($D5_{13}$ structure), and bcc NiAl in the $B2$ structure—were compared to the corresponding all-electron calculations. The structural properties and relative heats are in excellent agreement (better than 0.01 eV/atom), although the the pseudopotential calculated heats were consistently more bound by about 0.05 eV/atom.

APPENDIX B: FREE ENERGY CALCULATION

The statistical mechanics of an ordered homogeneous thermodynamically stable compound is complicated by the fact that various types of atomic defects must coexist in order to insure that stoichiometry and homogeneity of the material are maintained. To study the defect properties of homogeneous $NiAl_3$, a statistical mechanical model similar to the one developed for NiAl (Ref. 12) is used, but generalized to consider a binary system with four sublattices and stoichiometries other than 1:1.

At stoichiometry, the A atoms occupy the α sublattice and the B atoms occupy the β and γ sublattices with the λ sublattice vacant. For $NiAl_3$, the A and B atoms will correspond to the Ni and Al atoms, respectively, so that the α, β, γ, and λ sublattices correspond to the Ni, Al $8d$, Al $4c$, and interstitial sublattices, respectively. The number of defects is given by N_i^ν, where i refers to the type of defect (vacancy, antisite, or interstitial) and ν indicates the sublattice (α, β, γ, or λ). The number of A and B atoms is given by N_A and N_B, respectively. In terms of the number of defects, N_A and N_B may be expressed as

$$N_A=M^\alpha-N_B^\alpha-N_v^\alpha+N_A^\beta+N_A^\gamma+N_A^\lambda, \tag{B1}$$

$$N_B=Ms^\beta+M^\gamma-N_A^\beta-N_A^\gamma-N_v^\beta-N_v^\gamma+N_B^\alpha+N_B^\lambda, \tag{B2}$$

where M^α, M^β, and M^γ represent the number of α, β, and γ sites available.

With the introduction of a point defect, the energy and volume change by ε_i^ν and v_i^ν, respectively. For low concentrations of defects, which is the case close to stoichiometry and far away for the order-disorder temperature, we assume that ε_i^ν and v_i^ν are independent of the concentration; i.e., the defects are considered to be noninteracting. Such a noninteracting model allows us to write down an expression for the internal energy, volume, and configurational entropy. (The vibrational entropy is not considered in this model.) By minimizing the Gibbs free energy with respect to the number of point defects, N_i^ν, we obtain equations for the concentration of defects:

$$c_v^\alpha=\frac{M^\alpha}{M}\frac{e^{-\beta(\varepsilon_v^\alpha+\mu_A+Pv_v^\alpha)}}{1+e^{-\beta(\varepsilon_v^\alpha+\mu_A+Pv_v^\alpha)}+e^{-\beta(\varepsilon_B^\alpha+\mu_A-\mu_B+Pv_B^\alpha)}}, \tag{B3}$$

$$c_B^\alpha=\frac{M^\alpha}{M}\frac{e^{-\beta(\varepsilon_B^\alpha+\mu_A-\mu_B+Pv_B^\alpha)}}{1+e^{-\beta(\varepsilon_v^\alpha+\mu_A+Pv_v^\alpha)}+e^{-\beta(\varepsilon_B^\alpha+\mu_A-\mu_B+Pv_B^\alpha)}}, \tag{B4}$$

with similar expressions for the β and γ sublattices, and

$$c_A^\lambda=\frac{M^\lambda}{M}\frac{e^{-\beta(\varepsilon_A^\lambda-\mu_A+Pv_A^\lambda)}}{1+e^{-\beta(\varepsilon_A^\lambda-\mu_A+Pv_A^\lambda)}+e^{-\beta(\varepsilon_B^\lambda-\mu_B+Pv_B^\lambda)}}, \tag{B5}$$

$$c_B^\lambda=\frac{M^\lambda}{M}\frac{e^{-\beta(\varepsilon_B^\lambda-\mu_B+Pv_B^\lambda)}}{1+e^{-\beta(\varepsilon_A^\lambda-\mu_A+Pv_A^\lambda)}+e^{-\beta(\varepsilon_B^\lambda-\mu_B+Pv_B^\lambda)}}, \tag{B6}$$

for the λ sublattice. The chemical potentials $\mu_A(T,P,x)$ and $\mu_B(T,P,x)$ are Lagrange multipliers to ensure the conservation of A and B atoms. They are related to the Gibbs free energy by

$$G=U-TS+PV=\mu_AN_A+\mu_BN_B. \tag{B7}$$

From these equations, one obtains

$$\varepsilon_0 + P v_0 = \frac{M^\alpha}{M}\mu_A + \frac{M^\beta + M^\gamma}{M}\mu_B - \frac{M^\alpha}{M}k_B T \ln\left(1 - \frac{M}{M^\alpha}c_v^\alpha - \frac{M}{M^\alpha}c_B^\alpha\right) - \frac{M^\beta}{M}k_B T \ln\left(1 - \frac{M}{M^\beta}c_v^\beta - \frac{M}{M^\beta}c_A^\beta\right) - \frac{M^\gamma}{M}k_B T \ln\left(1 - \frac{M}{M^\gamma}c_v^\gamma - \frac{M}{M^\gamma}c_A^\gamma\right) - \frac{M^\lambda}{M}k_B T \ln\left(1 - \frac{M}{M^\lambda}c_A^\lambda - \frac{M}{M^\lambda}c_B^\lambda\right), \tag{B8}$$

where ε_0 and v_0 are the energy and volume, respectively, of the ideal system. The composition of the compound is given by

$$\frac{N_A}{N_B} = \frac{M^\alpha - N_B^\alpha - N_v^\alpha + N_A^\beta + N_A^\gamma + N_A^\lambda}{M^\beta + M^\gamma - N_A^\beta - N_A^\gamma - N_v^\beta - N_v^\gamma + N_B^\alpha + N_B^\lambda} = \frac{x}{1-x}, \tag{B9}$$

which guarantees the correct composition of the system.

The parameters ε_i^ν and v_i^ν can be obtained from first-principles calculations on supercells containing the defects. Once these parameters are available, the chemical potentials may be obtained by solving Eqs. (B9), (B8), and (B3)–(B6) as complicated functions of T, P, and x. Analytic expressions can be obtained at low temperatures and pressures.[12,19] Once the chemical potentials μ_A and μ_B are known, then all other quantities are available, including the free energy and defect formation energies.

Equations (B3)–(B6) for the defect concentration equations are described by energy barriers that must be thermally overcome in order to begin forming defects. These quantities, the defect formation energies, are given by

$$\Delta H_i^\nu = \varepsilon_i^\nu - \delta_{i,A}\mu_A + \delta_{\nu,\alpha}\mu_A - \delta_{i,B}\mu_B + (\delta_{\nu,\beta} + \delta_{\nu,\gamma})\mu_B, \tag{B10}$$

and depend on the chemical potentials μ_A and μ_B. The chemical potentials serve to describe the system in terms of the same number of A and B atoms. For example, creating a vacancy on the α sublattice requires an energy

$$\Delta H_v^\alpha = \varepsilon_v^\alpha + \mu_A, \tag{B11}$$

where ε_v^α describes the energy cost of creating the defect and μ_A the energy of adding an A atom to maintain the correct concentration.

[1] Zs. Kovács, L. Kövér, P. Weightman, D. Varga, R. Sajinés, J. Pálinkás, G. Margaritondo, and H. Adachi, Phys. Rev. B **54**, 8501 (1996).

[2] J.C. Fuggle, F.U. Hillebrecht, R. Zeller, Z. Zolnierek, P.A. Bennett, and Ch. Freiburg, Phys. Rev. B **27**, 2145 (1982).

[3] A. Mansour, A. Dmitrienko, and V. Soldatov, Phys. Rev. B **55**, 15 531 (1997).

[4] A. Pasturel, C. Colinet, H. Paxton, and M. van Schilfgaarde, J. Phys.: Condens. Matter **4**, 945 (1992).

[5] G. Cubiotti, E.E. Krasovskii, O.V. Slobodyan, Yu.N. Kucherenko, and V.N. Antonov, J. Phys.: Condens. Matter **7**, 4865 (1995).

[6] D. Hackenbracht and J. Kübler, J. Phys. F: Met. Phys. **10**, 427 (1980).

[7] P.T. Andrews, S.C. Millar, G. Cubiotti, Yu. Kucherenko, A.N. Yaresko, and V.N. Antonov, J. Phys.: Condens. Matter **5**, 1935 (1993).

[8] N. Chetty, M. Weinert, T. Rahman, and J. Davenport, Phys. Rev. B **52**, 6313 (1995).

[9] S. Vosko, L. Wilk, and M. Nusair, Can. J. Phys. **58**, 1200 (1980).

[10] H. Monkhorst and J. Pack, Phys. Rev. B **13**, 5188 (1976).

[11] A.J. Bradley and A. Taylor, Philos. Mag. **23**, 1049 (1937).

[12] B. Meyer and M. Fähnle, Phys. Rev. B **59**, 6072 (1999).

[13] C. Fu, Phys. Rev. B **52**, 3151 (1995).

[14] M. Alatalo, M. Weinert, and R.E. Watson, Phys. Rev. B **57**, R2009 (1998).

[15] M. Alatalo, M. Weinert, and R.E. Watson, Phys. Rev. B **60**, 7680 (1999).

[16] N. Troullier and J.L. Martins, Phys. Rev. B **43**, 1993 (1991).

[17] L. Kleinman and D.M. Bylander, Phys. Rev. Lett. **48**, 1425 (1982).

[18] G.W. Fernando, J.W. Davenport, R.E. Watson, and M. Weinert, Phys. Rev. B **40**, 2757 (1989).

[19] J. Mayer, C. Elässer, and M. Fähnle, Phys. Status Solidi B **191**, 283 (1995).